

The Role of Phe82 and Phe351 in Auxin-Induced Substrate Perception by TIR1 Ubiquitin Ligase: A Novel Insight from Molecular Dynamics Simulations

Ge-Fei Hao, Guang-Fu Yang*

Key Laboratory of Pesticide & Chemical Biology of Ministry of Education, College of Chemistry, Central China Normal University, Wuhan, People's Republic of China

Abstract

It is well known that Auxin plays a key role in controlling many aspects of plant growth and development. Crystal structures of Transport inhibitor response 1 (TIR1), a true receptor of auxin, were very recently determined for TIR1 alone and in complexes with auxin and different synthetic analogues and an Auxin/Indole-3-Acetic Acid (Aux/IAA) substrate peptide. However, the dynamic conformational changes of the key residues of TIR1 that take place during the auxin and substrate perception by TIR1 and the detailed mechanism of these changes are still unclear. In the present study, various computational techniques were integrated to uncover the detailed molecular mechanism of the auxin and Aux/IAA perception process; these simulations included molecular dynamics (MD) simulations on complexes and the free enzyme, the molecular mechanics Poisson Boltzmann surface area (MM-PBSA) calculations, normal mode analysis, and hydrogen bond energy (HBE) calculations. The computational simulation results provided a reasonable explanation for the structure-activity relationships of auxin and its synthetic analogues in view of energy. In addition, a more detailed model for auxin and Aux/IAA perception was also proposed, indicating that Phe82 and Phe351 played a pivotal role in Aux/IAA perception. Upon auxin binding, Phe82 underwent conformational changes to accommodate the subsequent binding of Aux/IAA. As a result, auxin enhances the TIR1-Aux/IAA interactions by acting as a “molecular glue”. Besides, Phe351 acts as a “fastener” to further improve the substrate binding. The structural and mechanistic insights obtained from the present study will provide valuable clues for the future design of promising auxin analogues.

Citation: Hao G-F, Yang G-F (2010) The Role of Phe82 and Phe351 in Auxin-Induced Substrate Perception by TIR1 Ubiquitin Ligase: A Novel Insight from Molecular Dynamics Simulations. PLoS ONE 5(5): e10742. doi:10.1371/journal.pone.0010742

Editor: Bostjan Kobe, University of Queensland, Australia

Received: March 18, 2010; **Accepted:** April 28, 2010; **Published:** May 20, 2010

Copyright: © 2010 Hao, Yang. This is an open-access article distributed under the terms of the Creative Commons Attribution License, which permits unrestricted use, distribution, and reproduction in any medium, provided the original author and source are credited.

Funding: The research was supported in part by the National Basic Research Program of China (No. 2010CB126103) and the NSFC (No. 20925206 and 20932005). The funders had no role in study design, data collection and analysis, decision to publish, or preparation of the manuscript.

Competing Interests: The authors have declared that no competing interests exist.

* E-mail: gfyang@mail.ccnu.edu.cn

Introduction

As a pivotal plant hormone, auxin controls many aspects of plant growth and development [1–7] by modulating gene expression and, thus, leading to changes in cell division, expansion, and differentiation [8,9]. Indole-3-acetic acid (IAA) is the major naturally occurring auxin. In addition, several synthetic auxins have also been developed, including 2,4-dichlorophenoxyacetic acid (2,4-D), 1-naphthalene acetic acid (1-NAA), 2-methoxy-3,6-dichlorobenzoic acid (dicamba), 4-amino-3,5,6-trichloropicolinic acid (tordon or picloram), α -(*p*-chlorophenoxy) isobutyric acid (PCIB, an antiauxin), and so on (Figure 1) [10]. These chemically diverse molecules share two common characteristics: a planar aromatic ring and a side chain with a carboxyl group. Although auxin is known as one of the most important “signaling messengers” in the plant kingdom, the detailed action mechanism of auxin with its receptor remains one of the most interesting questions in plant biology.

Auxin binding protein 1 (ABP1) is the first protein thought to be a possible auxin receptor [11–16]. A potential physiological mechanism for auxin-ABP1-induced changes of the plasma membrane has recently been found by a molecular modeling study [17], but the detailed physiological role of this protein in auxin-mediated signal regulation has not been realized [12,18]. In addition, some aspects of auxin-regulated transcription are

well understood [19,20]. For example, two families of transcription factor proteins have been identified in the response of transcription: auxin response factors (ARFs) and Auxin/Indole-3-Acetic Acid (Aux/IAA) transcriptional repressor proteins [21–26]. Recently, Transport inhibitor response 1 (TIR1), the F-box protein subunit of the ubiquitin-ligase complex (SCF^{TIR1}), was identified as a true auxin receptor. It was also revealed that auxin binds directly to TIR1 and increases the binding between Aux/IAA and TIR1 [27,28]. Most importantly, a series of crystallographic structures of TIR1, auxin, and Aux/IAA complex were very recently reported, which revealed that auxin, acting as ‘molecular glue’, enhanced TIR1-Aux/IAA interactions by filling a hydrophobic cavity at the interface between TIR1 and Aux/IAA [26,29,30]. Actually, structural analysis of TIR1 in complex with auxin and the Aux/IAA protein uncovered the pivotal role of auxin on the degradation of Aux/IAA proteins that actually activated ARF-induced DNA transcription [14,31–34]. Thus, the first structural model of a plant hormone receptor had been proposed. However, the detailed mechanism of the dynamic conformational changes that key residues of TIR1 undergo during auxin and substrate perception by TIR1 is still unknown.

In the present study, various computational techniques, including molecular dynamics (MD) simulations on complexes

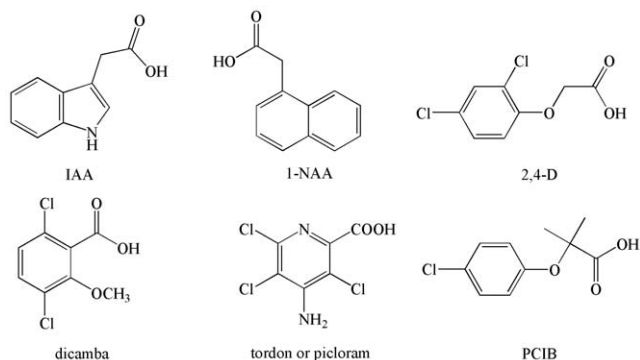


Figure 1. Chemical structures of IAA and some synthetic auxins.

doi:10.1371/journal.pone.0010742.g001

and the free enzyme, the molecular mechanics Poisson Boltzmann surface area (MM-PBSA) calculations, normal mode analysis (NMA), and hydrogen bond energy (HBE) calculations were integrated to uncover the detailed molecular mechanism of the Aux/IAA perception process. The crystal structures of TIR1 in complex with IAA; 2,4-D; and 1-NAA were used as the initial structures for MD simulations which were carried out to investigate the stability of protein conformation, especially, the conformational flexibility of Loop-2 of TIR1 and its relation to the binding. In addition, a reasonable explanation for the structure-activity relationships of auxin and its analogues was provided by the results of MM-PBSA and NMA calculations. Based on the results of computational simulation and energy calculation, a detailed Aux/IAA perception model was proposed, which explained the key roles of co-factor inositol hexakisphosphate (InsP6) and residues Phe82 and Phe351.

Methods

System Preparation

The initial structures of IAA; 2,4-D; and 1-NAA-TIR1 complexes used in our computational studies came from the X-ray crystal structures (pdb entry: 2P1Q, 2P1N, and 2P1O) in the Protein Data Bank [30]. One crystallization water molecule involved a water-bridge between residues and ligands was retained for each system, and other crystallization water molecules were removed. Standard Amber ff99 force field was assigned to the protein, and the general AMBER force field (gaff) was assigned to the ligands including the co-factor InsP6 [35–37]. The partial atomic charges of ligands were calculated using the am1-bcc method implemented in the Antechamber module of the Amber8 package [38]. Default protonation states were set to the ionizable residues at $pH = 7$. Considering the overall electroneutrality of the system, an appropriate number of Na^+ ions were added to the most electronegative areas around the protein. Then, each system was embedded in the truncated octahedron box of TIP3P water molecules with a 8.0 Å buffer along each dimension [39], resulting in a system with ~88000 atoms. To avoid edge effects, periodic boundary conditions were applied in all calculations.

For each system, energy minimizations and MD simulations were performed using the Sander module of the Amber3 program. First, the complex was frozen and the solvent molecules and counterions were allowed to move during a 5000-step minimization (2000 steps of the steepest descent and 3000 steps of the conjugated gradient minimization). Then, all atoms were energy-

minimized with 10000 steps (5000 steps of the steepest descent and 5000 steps of the conjugated gradient minimization). After the minimization stage, the system was slowly heated from $T = 10$ to 300 K in 40 ps and equilibrated in 160 ps before a sufficiently long MD simulation at room temperature. Finally we run the MD simulations of each system at 1 atm and 300 K for 2 ns or longer to make sure that we obtained a stable MD trajectory for each of the simulated structures. The time step used for the MD simulations was set to 2.0 fs and the coordinates were collected every 1 ps. In the simulation, the covalent bonds to hydrogen atoms were constrained using the SHAKE algorithm [40]. The Particle Mesh Ewald (PME) method was employed to calculate long-range electrostatic interactions [41,42]. The cutoff distances for the long-range electrostatic and van der Waals energy terms were set at 10.0 Å.

MM-PBSA Calculation

The calculations for the binding free energies of each system were based upon snapshots taken from a single trajectory of the complex MD simulation. A total of 100 snapshots were taken from the last 0.5 ns trajectory with an interval of 5 ps for each system. The counterions and water molecules (waters related to the crucial hydrogen bond were not included) were stripped. The MM-PBSA approach implemented in the Amber8 program was used to calculate the relative binding free energies of ligands to the TIR1 protein. The detailed description of this method can be found elsewhere [43]. Generally, the protein-ligand binding free energy was calculated using the following equations:

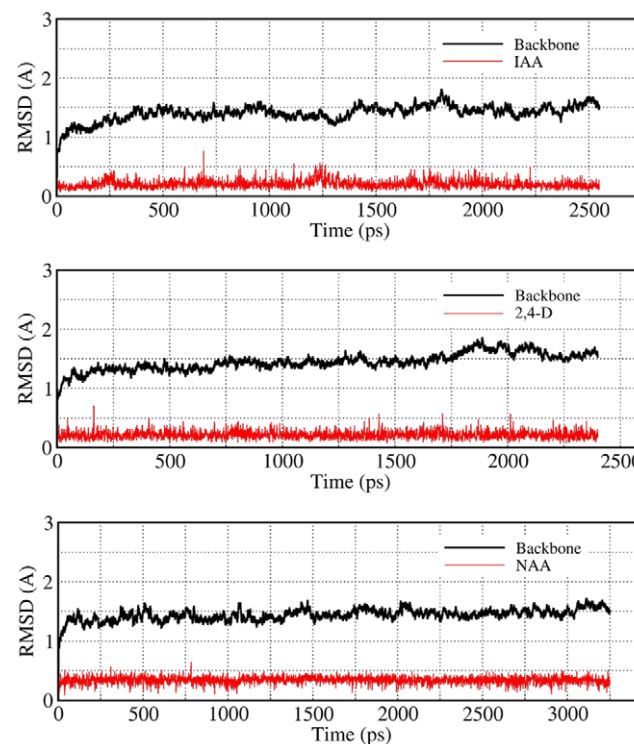


Figure 2. RMSD plots of the complexes during MD-simulations. RMSD of the backbone was calculated according to the coordinates of the main chain $C\alpha$ atoms shown in black and the RMSD of the ligand was calculated according to the coordinates of all atoms of the ligand shown in red.

doi:10.1371/journal.pone.0010742.g002

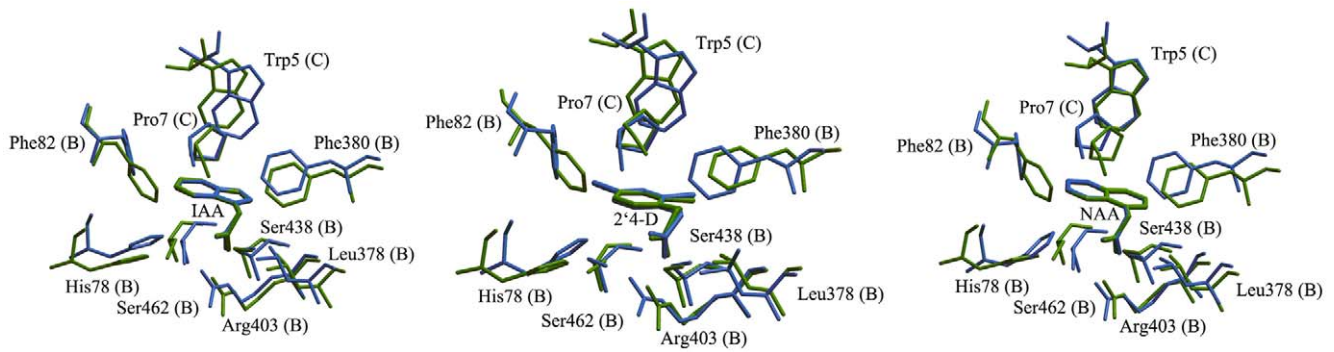


Figure 3. Superimposition between the MD-simulated structures and the X-ray structures. Average structures from the last 0.5 ns of the MD simulations of the complexes were superimposed on the X-ray structures via the heavy atoms of the active site. Heavy atoms of the ligands and selected neighboring residues less than 4 Å are shown in stick for the (a) IAA complex (b) 2, 4-D complex, and (c) 1-NAA complex. The crystal structure is shown in green and the MD structure is shown in blue.
doi:10.1371/journal.pone.0010742.g003

$$\Delta G_{\text{bind}} = \Delta G_{\text{complex}} - (\Delta G_{\text{receptor}} + \Delta G_{\text{ligand}}) \quad (1)$$

$$\Delta G_{\text{solv}} = \Delta G_{\text{PB}} + \Delta G_{\text{np}} \quad (4)$$

where $\Delta G_{\text{complex}}$, $\Delta G_{\text{receptor}}$, and ΔG_{ligand} are the free energies of the complex, the receptor, and the ligand, respectively. Each can be evaluated as follows:

$$\Delta G_{\text{np}} = \gamma \text{SASA} + \beta \quad (5)$$

$$\Delta G_{\text{complex/receptor/ligand}} = \Delta E_{\text{MM}} + \Delta G_{\text{solv}} - T\Delta S \quad (2)$$

$\Delta G_{\text{complex/receptor/ligand}}$ was evaluated as a sum of the changes in the molecular mechanical (MM) gas-phase binding energy (ΔE_{MM}), solvation free energy (ΔG_{solv}), and entropy term ($-T\Delta S$). The molecular mechanics gas-phase binding energy (ΔE_{MM}) can be calculated by equation 3, where ΔE_{val} , ΔE_{cle} and ΔE_{vdw} represent the internal energy contribution from bonds, angles and torsions, electrostatic and van der Waals interactions, respectively. The solvation energy ΔG_{solv} can also be separated into two parts (equation 4): ΔG_{PB} (the electrostatic contribution to the solvation free energy) and ΔG_{np} (nonpolar contribution to the solvation free energy). The DelPhi program [44] with PARSE radii [45] was used to evaluate ΔG_{PB} . The grid spacing of the cubic lattice was 0.5 Å. The dielectric constants used for the interior and exterior were 1 and 80, respectively, and 1000 iterations were performed for the linear PB equation. The nonpolar contribution to the solvation free energy can be determined using the function of the solvent accessible surface area (SASA) [45,46], with parameters $\gamma = 0.00542 \text{ kcal}/\text{Å}^2$ and $\beta = 0.92 \text{ kcal/mol}$ (equation 5).

$$\Delta E_{\text{MM}} = \Delta E_{\text{val}} + \Delta E_{\text{cle}} + \Delta E_{\text{vdw}} \quad (3)$$

In this work, we calculated the binding free energies of each complex using the MM-PBSA method. The conformational entropies are important contributions to the receptor-ligand binding. Therefore, the NMA was performed to estimate the conformational entropy change upon ligand binding using the nmode program in Amber8 [47]. Each snapshot was fully minimized until the root-mean-square of the elements of the gradient vector was less than $1 \times 10^{-4} \text{ kcal} \cdot \text{mol}^{-1} \text{ Å}^{-1}$. Due to the high computational cost, residues around the ligand (less than 8 Å) were used to estimate the contribution of the entropies of association and other residues were removed from each snapshot. The same strategy had been successfully applied elsewhere [48]. The calculation error bars are standard errors (SE) calculated using equation 6, where STD is standard deviation and N is the number of trajectory snapshots used in the calculation.

$$\text{SE} = \frac{\text{STD}}{\sqrt{N}} \quad (6)$$

Hydrogen bond energy calculation

Hydrogen bonds are formed according to both distance and orientation. If the distance between the donor (D) and acceptor (A)

Table 1. Calculated and Experimental Energetic Data (kcal/mol) at T = 298.15 K.

	ΔE_{ele}	bcc Charge	ΔE_{vdw}	ΔE_{gas}	ΔG_{solv}	ClogP	ΔG_{PB}	$-T\Delta S$	ΔG_{cal}	ΔG_{exp}^a
IAA	23.92 (0.72)	-0.84	-25.28 (0.28)	-1.36 (0.68)	-23.03 (0.62)	1.08	-24.39 (0.48)	14.55 (0.53)	-9.84	-9.45
2, 4-D	50.40 (0.92)	-0.56	-29.12 (0.28)	21.29 (0.89)	-42.78 (0.85)	2.69	-21.50 (0.66)	13.85 (0.52)	-7.65	-8.00
1-NAA	54.65 (0.70)	-0.57	-28.23 (0.26)	26.42 (0.67)	-49.98 (0.62)	2.53	-23.56 (0.48)	15.60 (0.51)	-7.96	-8.04

a. The experimental values ΔG_{exp} were derived from the experimental IC_{50} values reported in Ref [27].
doi:10.1371/journal.pone.0010742.t001

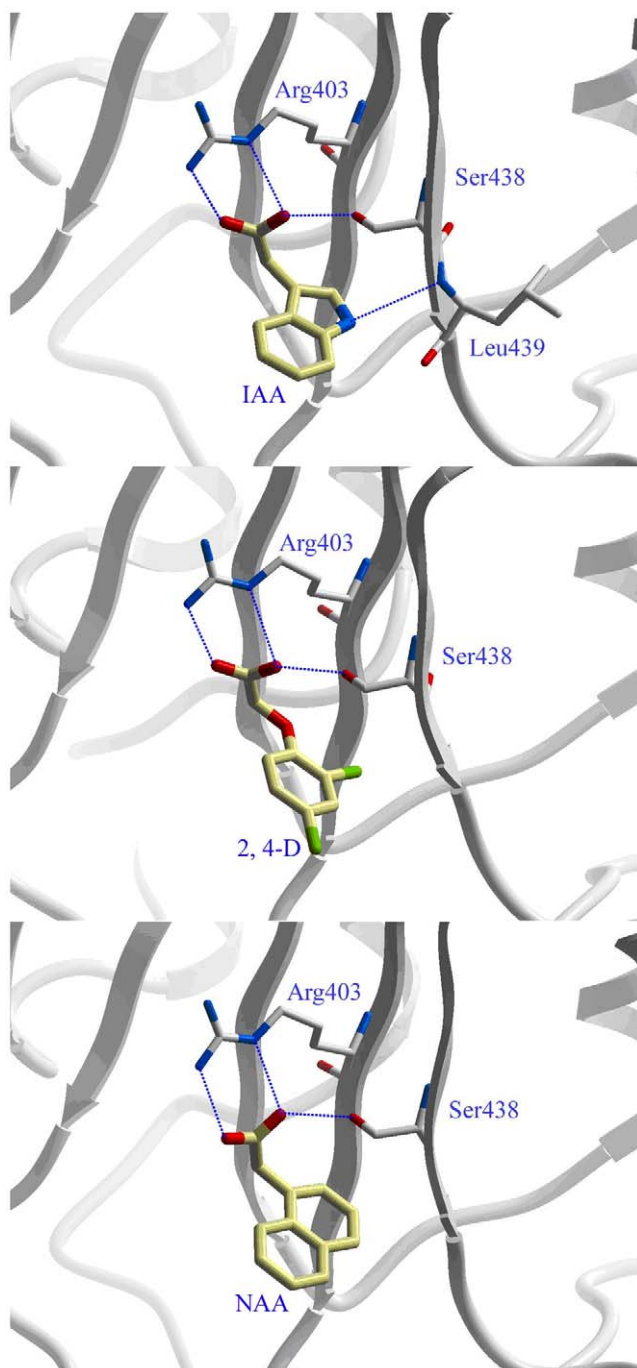


Figure 4. Hydrogen-bonding interaction of IAA, 2,4-D, NAA with their receptor. The H-bond distance was taken from an averaged snapshot selected from the MD simulation. doi:10.1371/journal.pone.0010742.g004

is shorter than 3.5 Å and the degree of the angle D–H...A ranges from 120° to 180°, D, H, and A with a D–H...A conformation will be considered a hydrogen bond. Generally speaking, hydrogen bonds with distance between H and A less than 2 Å are considered very strong [49]. In this work, the Ptraj module of Amber8 program was used for hydrogen bond analysis. To further understand the overall strength of the hydrogen bonding network, the HBE was calculated using the empirical HBE equation implemented in the Autodock 3.05 program [50]. The general

HBE equation is

$$\text{HBE}(r) \approx 5\epsilon r_{\text{eqm}}^{12}/r^{12} - 6\epsilon r_{\text{eqm}}^{10}/r^{10} \quad (7)$$

where r is the distance between the donor hydrogen atom (H) and acceptor atom (A), r_{eqm} is the equilibrium internuclear separation between H and A, and ϵ is the energy well depth at r_{eqm} . The parameters r_{eqm} and ϵ of the hydrogen bond acceptor were assigned by default.

Results and Discussion

Validation of the computational models

To evaluate the stability of the three complexes during the MD simulation, root-mean-square deviation (RMSD) values of protein backbone atoms and the ligands related to the initial X-ray crystal structure in the whole MD trajectory were examined, as shown in Figure 2. This clearly indicated the RMSD values of the protein backbone atoms and ligand atoms were always kept around 1.5 Å and 0.4 Å respectively, which showed that the MD-simulated binding models were stable. Therefore, to acquire an atomic view of the difference between the MD-simulated structures and crystal structures, the active site residues located within 4 Å of the ligand in the MD-simulated complex were superimposed with that of the crystal complex. As shown in Figure 3, most of the residues in the MD-simulated complex took almost the same orientation as in the crystal complex. Only residue Phe82 in the MD-simulated complex was found to display conformational changes compared to the crystal complex, which may be attributed to the flexibility of the binding cavity. Although, other conformations may be possible for Phe82 and it cannot be excluded that the conformational change of Phe82 is responsible for the binding of Aux/IAA (the role of Phe82 will be discussed below). Most importantly, however, the conformations of the ligands in the MD-simulated complex and the crystal complex are almost the same. The RMSD values based on the heavy atoms of the active site for IAA; 2,4-D; and 1-NAA were 0.07 Å, 0.19 Å, and 0.09 Å, respectively. For the subsequent energy analysis, we saved a total of 100 snapshots from a stable MD trajectory of the last 500 ps, *i.e.* one structure every 5 ps, for each MD-simulated complex.

To further evaluate the reliability of these MD-simulated models, the binding affinity of IAA; 2,4-D; and 1-NAA with TIR1 were estimated by performing MM-PBSA calculations based on the single-trajectory MD simulations. The calculation results were compared with the experimental data, as summarized in Table 1. The experimental data (ΔG_{exp}) were estimated approximately from the reported IC₅₀ values [27] by the equation $\Delta G \approx -RT \ln IC_{50}$. As shown in Table 1, the calculated binding free energies (ΔG_{cal}) were −9.84 kcal/mol, −7.65 kcal/mol, and −7.96 kcal/mol for IAA; 2,4-D; and 1-NAA, respectively. The absolute values of the calculated binding free energies not only exhibited a remarkable level of agreement with the experimental values of 9.45 kcal/mol, −8.00 kcal/mol, and −8.04 kcal/mol for IAA; 2,4-D; and 1-NAA respectively (the difference is less than 0.40 kcal/mol), they also had a consistent qualitative order (IAA > 1-NAA > 2,4-D) with the experimental results. These results suggested the MD-simulated models and the computational protocol tested in this study were reliable.

Analysis of structure-activity relationships in view of energy

It is well known that hydrogen bonds play a pivotal role in protein-ligand interaction and make a great contribution to the

Table 2. Hydrogen bond networks of the complexes.

Ligand	TIR1		% ^a	Maximum Distance	Minimum Distance	Average Distance	HBEs ^c	THBE ^d
	Acceptor	Donor						
IAA	IAA: HN	LEU439: O	93.8	3.51	1.66	2.16	-0.47	-5.05
	IAA: O2	ARG403: HH21	100.0	2.40	1.55	1.78	-1.69	
	IAA: O3	SER438: HG	99.9	3.98	1.43	1.78	-1.79	
	IAA: O3	ARG403: HE	99.9	2.82	1.54	1.89	-1.11	
2,4-D	24-D: O2	ARG403: HE	99.6	2.78	1.58	1.86	-1.26	-3.25
	24-D: O1	ARG403: HH21	99.6	2.96	1.61	1.92	-1.01	
	24-D: O2	SER438: HG	95.6	4.12	1.45	2.00	-0.98	
1-NAA	NAA: O1	ARG403: HH21	100.0	2.78	1.56	1.82	-1.45	-3.73
	NAA: O2	ARG403: HE	99.8	3.09	1.60	1.94	-0.92	
	NAA: O2	SER438: HG	99.6	3.61	1.50	1.89	-1.25	
	NAA: O2	ARG403: HH21	70.8	3.78	1.76	2.57	-0.12	

^aOccupancy of hydrogen bonds (The occupancy >70% were listed).

^bHydrogen bond distance (Å).

^cHydrogen bond energy (kcal/mol), calculated according to $HBE(r) \approx 5\epsilon r_{eqm}^{12}/r^{12} - 6\epsilon r_{eqm}^{10}/r^{10}$, the parameters: $r_{eqm} = 1.43 \text{ \AA}$, $\epsilon = 5 \text{ kcal/mol}$. We calculated the HBE of every snapshot of the MD simulation and then took the average value.

^dTotal hydrogen bond energy (kcal/mol). The total HBE value is the average of the HBE values calculated by using the instantaneous distances in all of the snapshots. doi:10.1371/journal.pone.0010742.t002

total binding affinity. Therefore, we carefully analyzed the hydrogen bond networks during the whole MD simulation. As shown in Figure 4, Arg403 and Ser438 formed several hydrogen bonds with the carboxyl group of the ligands. In addition, the nitrogen atom on the indole ring of IAA formed a hydrogen bond with the side chain of Leu439. To understand the overall strength of the hydrogen bonding network in the MD simulation, we calculated the HBE of each simulated hydrogen bond using the empirical HBE equation. As shown in Table 2, the hydrogen bond occupancy rate and hydrogen bond distance always determine the hydrogen bond strength. Higher occupancy and shorter distance always result in lower HBE. IAA formed much stronger hydrogen bond interactions with the protein than 2,4-D and 1-NAA. Interestingly, the order of HBE (IAA>1-NAA>2,4-D) was in accordance with the strength of the binding free energies of the ligands, suggesting the hydrogen bonding interactions greatly contributed to the biological activity of auxin and its analogues.

It is very interesting to examine the interaction differences of IAA; 2,4-D; and 1-NAA with the receptor in view of energy. As shown in Table 1, the van der Waals interaction (-25.28 kcal/mol) between IAA and the TIR1-Aux/IAA complex is a little smaller than that of 2,4-D and 1-NAA (-29.12 kcal/mol and -28.23 kcal/mol, respectively). Due to the highly electronegative charges on the InsP6, the electrostatic interactions make unfavorable contribution to ligand binding. The long range negative electric exclusion energy to IAA is 23.92 kcal/mol, which is much smaller than that of 2,4-D and 1-NAA (50.40 and 54.65 kcal/mol, respectively). Therefore, IAA should have much better binding affinity in gas than 2,4-D and 1-NAA. However, because of the low solvation free energy (-23.03 kcal/mol), IAA only has a slightly better binding affinity than 2,4-D and 1-NAA. As for the entropic change, the three systems have very similar effects with values of 14.55, 13.85, and 15.60 kcal/mol for IAA; 2,4-D; and 1-NAA, respectively. To further investigate the differences between electrostatic and solvation effects on the protein-ligand interactions, the partial charges on the carboxyl oxygen atoms and the ClogP value of each ligand were compared.

As aforementioned, the carboxyl oxygen atoms of the ligands acted as acceptors to form hydrogen bonds with Arg403 and Ser438. Therefore, the partial charges on the carboxyl oxygen atoms should be very important to the strength of hydrogen bonds. As shown in Table 1 and Figure 5, the carboxyl oxygen atoms on IAA are more negative (-0.84) than that of 2,4-D (-0.56) and 1-NAA (-0.57), which might account for IAA forming stronger hydrogen bonds with residues Arg403 and Ser438 than 2,4-D and 1-NAA. However, compared with 2,4-D and 1-NAA, IAA has a ClogP value of only 1.08 (Table 1). As a result, IAA is more hydrophilic than 2,4-D and 1-NAA and thus has a high solvation energy. These results indicate the charges on the carboxyl oxygen atoms and the hydrophobic property of IAA should be considered in the molecular design of future auxin analogues.

Role of Phe82 and Phe351

From the above simulation results, we can conclude TIR1 has an important and unique characteristic: a mushroom-shaped structure with a rigid F-box motif as a 'stem' and a leucine-rich-repeat (LRR) domain as a 'cap'. This mushroom shape was always kept during the whole MD simulation process. However, two loops (loop2 and loop12) (shown in Figure 6A) in the LRR domain underwent interesting conformational changes during the MD

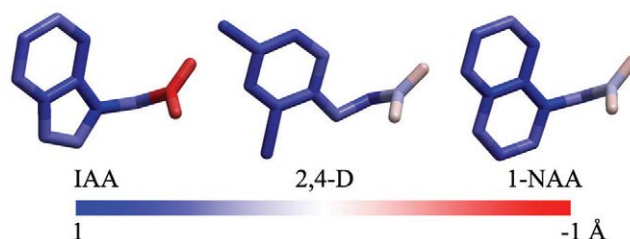


Figure 5. The comparison of partial charge on each atom. The color indicates the change of partial charges shown in the bottom bar. doi:10.1371/journal.pone.0010742.g005

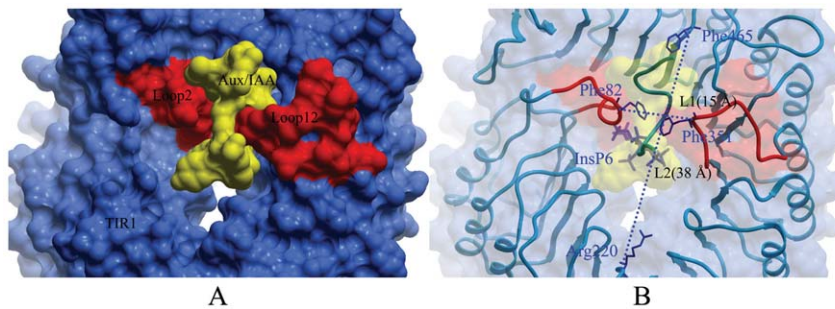


Figure 6. Architecture of the TIR1-LRR domain from the top view. The LRR domain is shown in blue and the two loops (loop2 and loop12) are shown in red. (A) Surface representation of the LRR domain. The substrate-binding concave groove is created by the closeness of loop2 and loop12, which nips the surface of the Aux/IAA. (B) The LRR domain are colored in blue and shown in the worm model. The distance between the C α atoms of Phe82 in Loop 2 and Phe351 in Loop 12 was defined as transverse distance, while the distance between the C α atoms of Arg220 and Phe465 was defined as lengthways distance.

doi:10.1371/journal.pone.0010742.g006

simulation process for auxin- and substrate-binding. As shown in Figure 6B, the changes in span distance of the LRR domain in the MD simulations of free TIR1 with or without InsP6 were analyzed to understand the conformational stabilization. As shown in Figure 7A and 7B, significant fluctuations of the span distance can be observed in both the transverse distance (varying from 10 Å to 17 Å) and lengthwise distance (varying from 36 Å to 41 Å) of the system without InsP6, compared with the transverse (from 12 to 16 Å) and lengthwise (from 35 to 39 Å) distances of the system with InsP6. This indicates the conformation of the LRR domain is more flexible without InsP6 binding. The results from X-ray crystal structures and the MD-simulations indicated that after InsP6 binding, the conformation of the LRR domain was partly stabilized by the complicated hydrogen-bonding network between InsP6 and the receptor (shown in Figure 7C). For example, the conserved residue Arg114 formed two hydrogen bonds with InsP6 and two hydrogen bonds with residue Asp81. So, Arg114 acted as a ‘bridge’ to link InsP6 and residue Asp81 together. The hydrogen bond interactions between Asp81 and Arg114 greatly contributed to the stabilization of Loop2. In addition, the conserved residue Arg403 formed hydrogen bonds with InsP6 and auxin. As a result, InsP6 and Auxin were linked together through the Arg403 ‘bridge’.

Most interestingly, our computational simulations indicated two residues, Phe82 and Phe351, underwent significant conformation-

al changes upon the sequential binding of auxin and Aux/IAA (such as Phe82 in Figure 8A). The side chain of Phe82 in Loop 2 had three kinds of orientations during the MD simulation for the free enzyme with two conformations occupied most of the simulation time (black line in Figure 8B). However, upon auxin binding, the side chain of Phe82 could be induced into a favorable orientation (red line in Figure 8B) to accommodate the subsequent binding of Aux/IAA. As a result of Aux/IAA binding, the side chain of Phe82 underwent an additional conformational change (blue line in Figure 8B). The side chain of Phe351 was relatively unstable during the MD simulations for the free enzyme and enzyme binding with auxin (black and red line in Figure 8C). The binding of Aux/IAA induced Phe351 to undergo a conformational change from an unstable to stable state (blue line in Figure 8C).

A proposed model for Aux/IAA perception

Based on the above computational simulations, we propose a new and detailed model for Aux/IAA perception, as depicted in Figure 9. Step 1, as a ‘conformational stabilizer’, the co-factor InsP6 binds to TIR1 to stabilize the local conformation of the LRR domain by forming hydrogen bonds with the surrounding residues. As a result of the binding of InsP6, a three-walled ‘groove’, the auxin-binding pocket, is assembled by Loop2, Loop12, and InsP6. Step 2, auxin enters this pocket and is grounded on the bottom of the ‘groove’. In addition to playing a

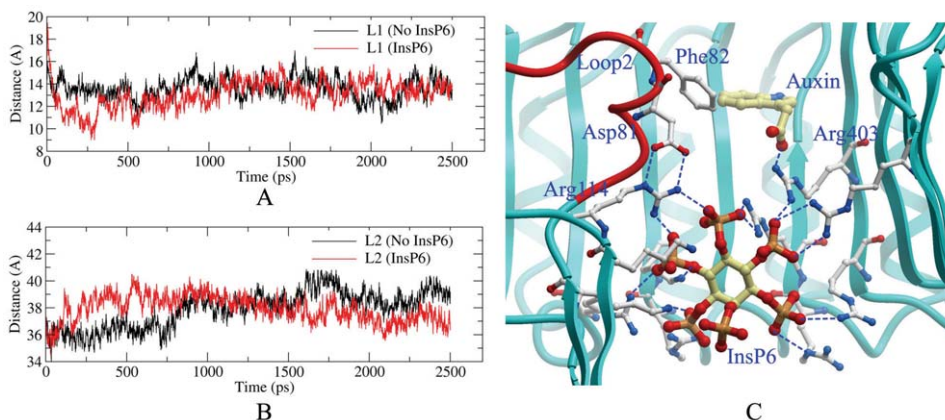


Figure 7. Changes of some key distances associated with InsP6 during MD simulations. The transverse distance changes (A) and the lengthways distance changes (B) of the LRR domain span along the MD simulation. The hydrogen bond networks around InsP6 (C).

doi:10.1371/journal.pone.0010742.g007

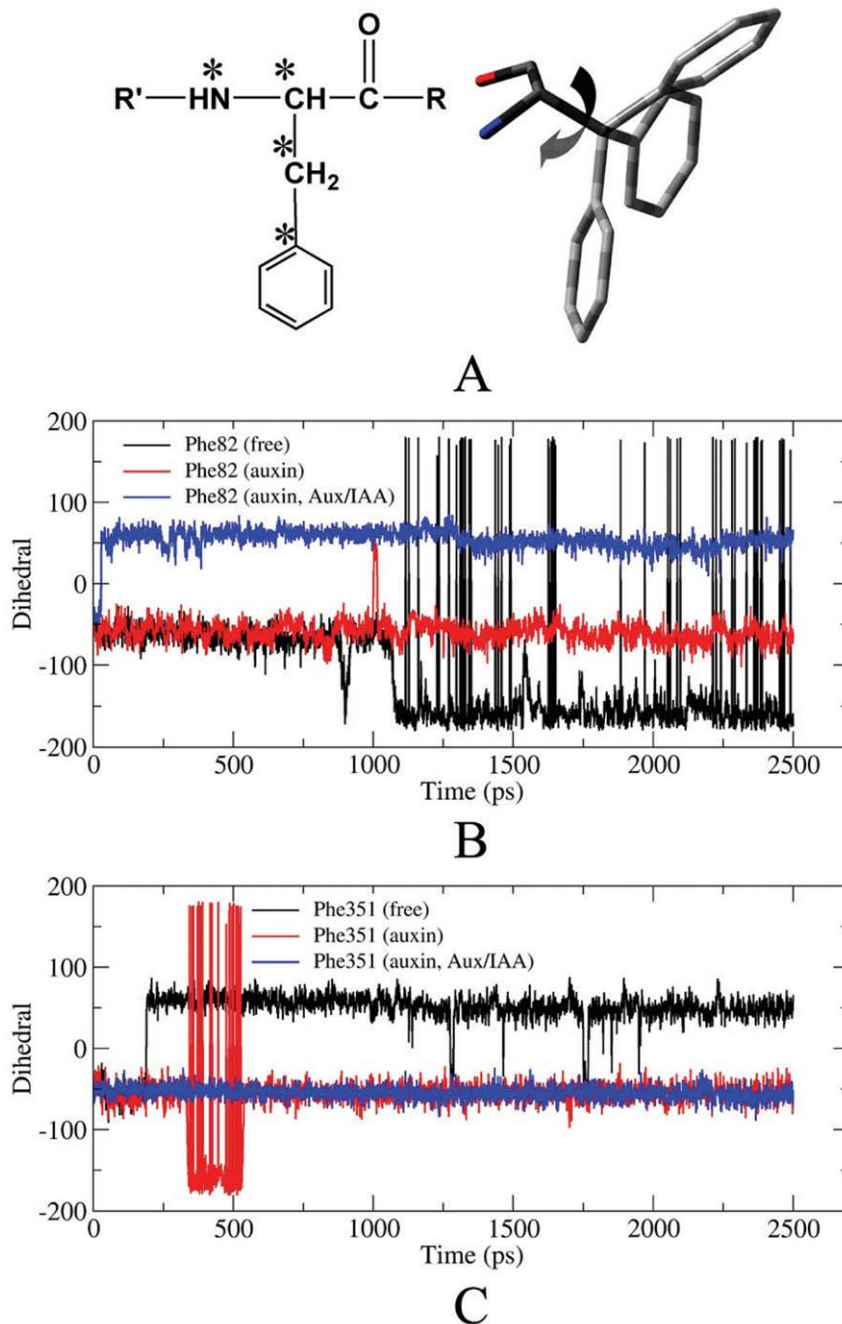


Figure 8. Changes of some key dihedral angles during MD simulations. Definition of dihedral angle for phenylalanine (A) and the comparison between the dihedral angle of Phe82 (B) and Phe351 (C) along the MD simulation in the free enzyme (black), enzyme with auxin (red), and enzyme with auxin and Aux/IAA (blue).

doi:10.1371/journal.pone.0010742.g008

role as a ‘molecular glue’ to increase the binding between Aux/IAA and TIR1, auxin also acts as a ‘conformation inducer’ leading Phe82 to undergo a conformational change to accommodate the subsequent binding of Aux/IAA. Step 3, Aux/IAA binds with TIR1. After the binding of Aux/IAA, Phe82 undergoes a further conformational change so that it reaches the optimum conformation for interacting with both auxin and Aux/IAA. At the same time, Phe351 acts as a ‘fastener’ to interact with Aux/IAA and prevent the substrate from leaving. Therefore, Phe82 and Phe351 play a pivotal role in Aux/IAA perception.

Conclusion

In summary, the detailed molecular mechanism of Aux/IAA perception was uncovered by performing a series of comparative molecular dynamics simulations, MM-PBSA free energy calculations, and hydrogen bond energy calculations. According to the results from free energy and hydrogen bond calculations, the structure-activity relationships of auxin and its synthetic analogues were uncovered in view of energy. In addition, a more detailed model for Aux/IAA perception was proposed based on the results of comparative MD simulations. This model indicates Phe82 and

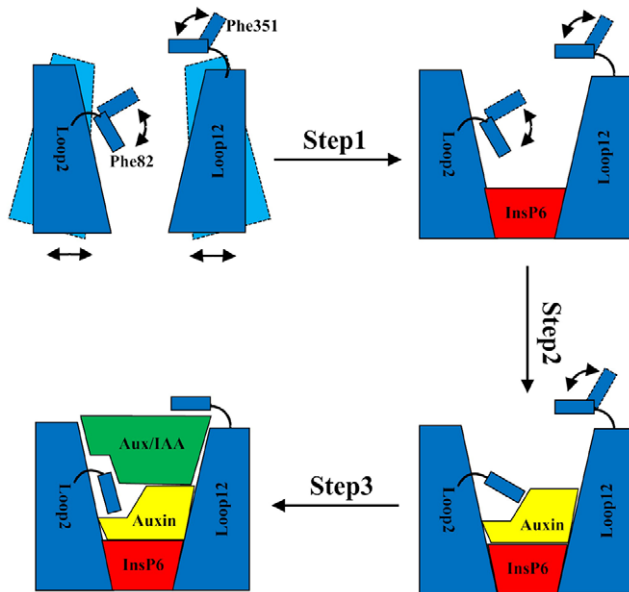


Figure 9. A proposed model for Aux/IAA perception.
doi:10.1371/journal.pone.0010742.g009

Phe351 play a pivotal role in Aux/IAA perception. Auxin acts not only as a ‘molecular glue’ to increase binding between Aux/IAA and TIR1, but also as a ‘conformation inducer’ triggering Phe82 to undergo conformational changes to accommodate the subsequent binding of Aux/IAA. At the same time, Phe351 also acts as a ‘fastener’ to further improve substrate binding. The structural and mechanistic insights obtained from the present study will provide valuable clues for the future design of promising auxin analogues.

Author Contributions

Conceived and designed the experiments: GFY. Performed the experiments: GFH. Analyzed the data: GFH. Wrote the paper: GFY.

References

- Perrot-Rechenmann C, Napier RM (2005) Auxins. *Vitam Horm* 72: 203–233.
- Woodward AW, Bartel B (2005) Auxin: regulation, action, and interaction. *Ann Bot* 95: 707–735.
- Teale WD, Paponov IA, Palme K (2006) Auxin in action: signalling, transport and the control of plant growth and development. *Nat Rev Mol Cell Biol* 7: 847–859.
- Dharmasiri N, Dharmasiri S, Jones AM, Estelle M (2003) Auxin action in a cell-free system. *Curr Biol* 13: 1418–1422.
- Hoecker U (2005) Regulated proteolysis in light signaling. *Curr Opin Plant Biol* 8: 469–476.
- Henriques R, Jang IC, Chua NH (2009) Regulated proteolysis in light-related signaling pathways. *Curr Opin Plant Biol* 12: 49–56.
- Callis J (2005) Plant biology: auxin action. *Nature* 435: 436–437.
- Ulmasov T, Hagen G, Guilfoyle TJ (1999) Activation and repression of transcription by auxin-response factors. *Proc Natl Acad Sci U S A* 96: 5844–5849.
- Gray WM, Kepinski S, Rouse D, Leyser O, Estelle M (2001) Auxin regulates SCF(TIR1)-dependent degradation of AUX/IAA proteins. *Nature* 414: 271–276.
- Taiz L, Zeiger E (2006) Auxin: The growth hormone. *Plant Physiology Online*. Sinauer Associates, Inc. Publishers. Chapter 19, Topic 19.1.
- Napier RM, David KM, Perrot-Rechenmann C (2002) A short history of auxin-binding proteins. *Plant Mol Biol* 49: 339–348.
- Woodward AW, Bartel B (2005) A receptor for auxin. *Plant Cell* 17: 2425–2429.
- Badescu GO, Napier RM (2006) Receptors for auxin: will it all end in TIRs? *Trends Plant Sci* 11: 217–223.
- Pieterse CM, Leon-Reyes A, Van der Ent S, Van Wees SC (2009) Networking by small-molecule hormones in plant immunity. *Nat Chem Biol* 5: 308–316.
- Friml J (2003) Auxin transport - shaping the plant. *Curr Opin Plant Biol* 6: 7–12.
- Woo EJ, Marshall J, Baulry J, Chen JG, Venis M, et al. (2002) Crystal structure of auxin-binding protein 1 in complex with auxin. *Embo J* 21: 2877–2885.
- Bertosa B, Kojic-Prodic B, Wade RC, Tomic S (2008) Mechanism of auxin interaction with Auxin Binding Protein (ABP1): a molecular dynamics simulation study. *Biophys J* 94: 27–37.
- Jones AM (1998) Auxin transport: down and out and up again. *Science* 282: 2201–2203.
- Kepinski S, Leyser O (2004) Auxin-induced SCFTIR1-Aux/IAA interaction involves stable modification of the SCFTIR1 complex. *Proc Natl Acad Sci U S A* 101: 12381–12386.
- Ramos JA, Zenser N, Leyser O, Callis J (2001) Rapid degradation of auxin/indoleacetic acid proteins requires conserved amino acids of domain II and is proteasome dependent. *Plant Cell* 13: 2349–2360.
- Hagen G, Guilfoyle T (2002) Auxin-responsive gene expression: genes, promoters and regulatory factors. *Plant Mol Biol* 49: 373–385.
- Tao LZ, Cheung AY, Wu HM (2002) Plant Rac-like GTPases are activated by auxin and mediate auxin-responsive gene expression. *Plant Cell* 14: 2745–2760.
- Reed JW (2001) Roles and activities of Aux/IAA proteins in Arabidopsis. *Trends Plant Sci* 6: 420–425.
- Rouse D, Mackay P, Stirnberg P, Estelle M, Leyser O (1998) Changes in auxin response from mutations in an AUX/IAA gene. *Science* 279: 1371–1373.
- Dreher KA, Brown J, Saw RE, Callis J (2006) The Arabidopsis Aux/IAA protein family has diversified in degradation and auxin responsiveness. *Plant Cell* 18: 699–714.
- Tiwari SB, Wang XJ, Hagen G, Guilfoyle TJ (2001) AUX/IAA proteins are active repressors, and their stability and activity are modulated by auxin. *Plant Cell* 13: 2809–2822.
- Dharmasiri N, Dharmasiri S, Estelle M (2005) The F-box protein TIR1 is an auxin receptor. *Nature* 435: 441–445.
- Kepinski S, Leyser O (2005) The Arabidopsis F-box protein TIR1 is an auxin receptor. *Nature* 435: 446–451.
- Zenser N, Ellsmore A, Leasure C, Callis J (2001) Auxin modulates the degradation rate of Aux/IAA proteins. *Proc Natl Acad Sci U S A* 98: 11795–11800.
- Tan X, Calderon-Villalobos LI, Sharon M, Zheng C, Robinson CV, et al. (2007) Mechanism of auxin perception by the TIR1 ubiquitin ligase. *Nature* 446: 640–645.
- Liscum E, Reed JW (2002) Genetics of Aux/IAA and ARF action in plant growth and development. *Plant Mol Biol* 49: 387–400.
- Hayashi K, Tan X, Zheng N, Hatate T, Kimura Y, et al. (2008) Small-molecule agonists and antagonists of F-box protein-substrate interactions in auxin perception and signaling. *Proc Natl Acad Sci U S A* 105: 5632–5637.
- Santner A, Calderon-Villalobos LI, Estelle M (2009) Plant hormones are versatile chemical regulators of plant growth. *Nat Chem Biol* 5: 301–307.
- Robert HS, Friml J (2009) Auxin and other signals on the move in plants. *Nat Chem Biol* 5: 325–332.
- Case DA, Darden TA, Cheatham TE, III, Simmerling CL, Wang J, et al. (2004) AMBER8. San Francisco, CA.: University of California.
- Wang J, Wolf RM, Caldwell JW, Kollman PA, Case DA (2004) Development and testing of a general amber force field. *J Comput Chem* 25: 1157–1174.
- Hornak V, Abel R, Okur A, Strockbine B, Roitberg A, et al. (2006) Comparison of multiple Amber force fields and development of improved protein backbone parameters. *Proteins* 65: 712–725.
- Jakalian A, Jack DB, Bayly CI (2002) Fast, efficient generation of high-quality atomic charges. AM1-BCC model: II. Parameterization and validation. *J Comput Chem* 23: 1623–1641.
- Jorgensen WL, Chandrasekhar J, Madura JD (1983) Comparison of simple potential functions for simulating liquid water. *J Chem Phys* 79: 926–935.
- Coleman TG, Mesick HC, Darby RL (1977) Numerical integration: a method for improving solution stability in models of the circulation. *Ann Biomed Eng* 5: 322–328.
- Darden T, York D, Pedersen L (1993) Particle mesh Ewald: An $N \cdot \log(N)$ method for Ewald sums in large systems. *J Chem Phys* 98: 10089–10092.

42. Essmann U, Perera L, Berkowitz ML (1995) A smooth particle mesh Ewald method. *J Chem Phys* 103: 8577–8593.
43. Kollman PA, Massova I, Reyes C, Kuhn B, Huo S, et al. (2000) Calculating structures and free energies of complex molecules: combining molecular mechanics and continuum models. *Acc Chem Res* 33: 889–897.
44. Honig B, Nicholls A (1995) Classical electrostatics in biology and chemistry. *Science* 268: 1144–1149.
45. Sitkoff D, Sharp KA, Honig B (1994) Accurate Calculation of Hydration Free Energies Using Macroscopic Solvent Models. *J Phys Chem* 98: 1978–1988.
46. Connolly ML (1983) Analytical molecular surface calculation. *J Appl Cryst* 16: 548–558.
47. Case DA, Cheatham TE, 3rd, Darden T, Gohlke H, Luo R, et al. (2005) The Amber biomolecular simulation programs. *J Comput Chem* 26: 1668–1688.
48. Kuhn B, Kollman PA (2000) Binding of a diverse set of ligands to avidin and streptavidin: an accurate quantitative prediction of their relative affinities by a combination of molecular mechanics and continuum solvent models. *J Med Chem* 43: 3786–3791.
49. Baker EN, Hubbard RE (1984) Hydrogen bonding in globular proteins. *Prog Biophys Mol Biol* 44: 97–179.
50. Morris GM, Goodsell DS, Halliday RS, Huey R, Hart WE, et al. (1998) Automated docking using a Lamarckian genetic algorithm and an empirical binding free energy function. *J Comput Chem* 19: 1639–1662.